geosciences

MDPI

Article

Neptunium(V) and Uranium(VI) Reactions at the Magnetite (111) Surface

Pieter Bots [1,2,*], Arjen van Veelen [1], J. Frederick W. Mosselmans [3], Christopher Muryn [4], Roy A. Wogelius [1] and Katherine Morris [1]

[1] Research Centre for Radwaste Disposal, School of Earth and Environmental Sciences, The University of Manchester, Oxford Road, Manchester, M13 9PL, UK; A.Van-Veelen@soton.ac.uk (A.V.); roy.wogelius@manchester.ac.uk (R.A.W.); katherine.morris@manchester.ac.uk (K.M.)

[2] Department of Civil and Environmental Engineering, University of Strathclyde, James Weir Building, 75 Montrose Street, Glasgow G1 1XJ, UK

[3] Diamond Light Source Ltd., Diamond House, Harwell Science & Innovation Campus, Didcot, OX11 0DE, UK; fred.mosselmans@diamond.ac.uk

[4] Photon Science Institute, School of Chemistry, The University of Manchester, Oxford Road, Manchester, UK, M13 9PL, UK; christopher.a.muryn@manchester.ac.uk

* Correspondence: pieter.bots@strath.ac.uk; Tel.: 00-44-141 3177

Received: 23 November 2018; Accepted: 1 February 2019; Published: 8 February 2019

Abstract: Neptunium and uranium are important radionuclides in many aspects of the nuclear fuel cycle and are often present in radioactive wastes which require long term management. Understanding the environmental behaviour and mobility of these actinides is essential in underpinning remediation strategies and safety assessments for wastes containing these radionuclides. By combining state-of-the-art X-ray techniques (synchrotron-based Grazing Incidence XAS, and XPS) with wet chemistry techniques (ICP-MS, liquid scintillation counting and UV-Vis spectroscopy), we determined that contrary to uranium(VI), neptunium(V) interaction with magnetite is not significantly affected by the presence of bicarbonate. Uranium interactions with a magnetite surface resulted in XAS and XPS signals dominated by surface complexes of U(VI), while neptunium on the surface of magnetite was dominated by Np(IV) species. UV-Vis spectroscopy on the aqueous Np(V) species before and after interaction with magnetite showed different speciation due to the presence of carbonate. Interestingly, in the presence of bicarbonate after equilibration with magnetite, an unknown aqueous NpO_2^+ species was detected using UV-Vis spectroscopy, which we postulate is a ternary complex of Np(V) with carbonate and (likely) an iron species. Regardless, the Np speciation in the aqueous phase (Np(V)) and on the magnetite (111) surfaces (Np(IV)) indicate that with and without bicarbonate the interaction of Np(V) with magnetite proceeds via a surface mediated reduction mechanism. Overall, the results presented highlight the differences between uranium and neptunium interaction with magnetite, and reaffirm the potential importance of bicarbonate present in the aqueous phase.

Keywords: uranium; neptunium; magnetite; surface; synchrotron; XAS; XPS; geodisposal; reduction

1. Introduction

Uranium and neptunium are important radionuclides in many aspects of the nuclear fuel cycle [1] and are often present in higher activity radioactive wastes requiring long term management and disposal strategies [2–4]. In most countries, the preferred long term management strategy of radioactive wastes is through their disposal in deep geological facilities [1]. Additionally, uranium is present in many contaminated land situations associated with, for example, reprocessing and mining activities [5–8]. Understanding the environmental behaviour and mobility of these actinides is

essential to underpin remediation strategies and safety assessments, and due to the prevalence of Np(V) in oxidized environments, Np could be a credible analogue for investigation of plutonium geochemistry.

In natural and engineered environments iron oxide minerals are ubiquitous [9] and have the potential to affect the mobility of radionuclides significantly through both incorporation and surface complexation processes [10–21]. In aerobic environments the redox states of the actinides (U, Np and Pu) are dominated by relatively soluble hexa- and pentavalent species, while under anoxic and progressively more reducing conditions, poorly soluble tetra- and trivalent species dominate [22]. Moreover, under reduced environments, magnetite ($Fe^{(II)}Fe^{(III)}{}_2O_4$) will be a significant iron oxide phase present in many geological disposal situations [9] and form as a corrosion product from zero valent iron in construction materials and stored wastes. Magnetite has been shown to affect the mobility of uranium [12,17,23–27], neptunium [16,28] and plutonium [13,17] through Fe(II) oxidation coupled to reduction of these actinides to less soluble (tri- and) tetravalent species including incorporation (U) and adsorption (U, Np, Pu) processes. It is postulated that the reduction of U(VI) occurs concurrently to oxidation of magnetite to maghemite [23,29,30]. This was observed for U(VI) interactions with magnetite surfaces [23,29,30] which reportedly occurs through the initial adsorption and subsequent reduction of adsorbed U(VI) to pentavalent uranium (U(V)) coupled with the oxidation of Fe(II) to Fe(III) [26]. On the surface of magnetite, U(V) subsequently disproportionates to U(IV) and U(VI) [31–34] and forms as a final reduction product either surface bound U^{4+} (at low surface coverage) or nanoparticulate uraninite (UO_2) (at elevated surface coverage) [24]. Conversely, in the case that U(V) incorporates into the structure of magnetite, it has been shown that this disproportionation to U(IV) and U(VI) is inhibited [18,21]. Finally, the U(VI) reduction rates and extent of reduction to U(IV) show a strong dependency on the stoichiometry of magnetite (Fe(II)/Fe(III)) [23] and are inhibited by aqueous bicarbonate through the formation of uranyl carbonate (surface) complexes [27,35].

The interaction of Np(V) with magnetite surfaces reportedly occurs through the initial adsorption of Np(V) followed by the reduction to surface Np^{4+} or nanoparticulate NpO_2 species [16,28,35]. In the case of plutonium, it is postulated that aqueous plutonium species (e.g., Pu^{4+} and PuO_2^{+}) interact with redox active (magnetite) and inactive (e.g., goethite and montmorillonite) mineral surfaces through adsorption followed by reduction to tetravalent and trivalent plutonium [13,17,36,37]. Interestingly, no detailed information is available on the mechanisms of Np(V) reduction on magnetite surfaces, specifically on the influence of bicarbonate species in solution on these mechanisms.

In this study, we aimed to provide a direct comparison of the interactions of actinide species (specifically U(VI) and Np(V)) with magnetite in order to obtain detailed information on their mechanisms of interaction including the influence of carbonate on these mechanisms. To achieve this we performed experiments on U(VI) and Np(V) interactions with single crystal magnetite with near-atomically flat (111) crystal faces to enable surface specific analyses of these mechanisms. We used two surface sensitive X-ray techniques (grazing incidence X-ray absorption spectroscopy (GI-XAS) and X-ray photoemission spectroscopy (XPS)) to obtain detailed information on the mechanisms of interaction of U(VI) and Np(V) with magnetite (111) surfaces.

2. Materials and Methods

All experiments were performed in an anaerobic chamber with solutions that were purged with argon gas. Single (near-)stoichiometric, natural magnetite crystals of 10 by 10 by 0.5 mm with the (111) crystal face polished were purchased from SurfaceNet GmbH, Germany. The crystals were used in the experiments as received. In total 4 experiments were performed at pH 7 in different buffer systems. The buffer solutions used were: 10 mM 3-(N-morpholino)propanesulfonic acid (MOPS); and 5 mM $NaHCO_3$. Two experiments were performed in buffer solutions (with either MOPS or $NaHCO_3$ buffers) with 10 ppm (42 μM) depleted uranium (as $U(VI)O_2^{2+}$) (U MOPS and U $NaHCO_3$). A second set of two experiments was performed in the same buffer solutions with 6 ppm (25 μM) neptunium-237 as $Np(V)O_2^{+}$ (Np MOPS and Np $NaHCO_3$) [38].

The 5 mM $NaHCO_3$ and 10 mM MOPS buffer solutions were prepared by dissolving MOPS or $NaHCO_3$ in 18.2 MΩ in a controlled atmosphere (CO_2 free anaerobic COY chamber) and the pH was adjusted to 7 using NaOH or HCl, respectively. The experiments were spiked with 600 ppm (2.5 mM) UO_2^{2+} (in ~6 mM HCl) or 20 kBq/ml (3 mM) $Np(V)O_2^+$ (in ~15 mM HCl, obtained from LEA-Cerca) stocks. At this stage magnetite single crystals were added to the buffer solutions and reacted for 14 days to ensure that the interaction of the actinides with the magnetite had completed [39]. Additionally, U(VI) and Np(V) spiked buffer solutions without magnetite were retained throughout the experiment to determine any removal of U(VI) and Np(V) from solution due to oversaturation. After 14 days, the magnetite crystals were removed from the aqueous phase and placed on aluminium holders with a Kapton cover and placed inside sealed PP bags and stored in a Kilner jar within the anaerobic chamber until further analyses (GI-XAS and XPS). Additionally, after 14 days, the aqueous phase of all buffer solutions was filtered through 0.2 μm nylon syringe filters and analysed for total uranium using an Agilent 7500cx ICP-MS and for neptunium using a Tri-Carb 2800tr liquid scintillation counter (LSC). The neptunium solution phases from experiments before and after reaction with magnetite single crystals were also analysed for UV-Vis spectroscopy on a Jenway 6850 spectrophotometer using a quartz cuvette to assess the speciation of aqueous neptunium in solutions equilibrated with magnetite or in the absence of magnetite. Combined, UV-Vis spectroscopy and electroplating followed by α- spectroscopy confirmed that the Np experiments were performed at 6 ppm (25 μM) NpO_2^+. Interestingly, the (3 mM) Np(V) stock also had ultra-trace concentrations (several μM) of $^{239,240}Pu$ present resulting in estimated concentrations of several ppb (tens of nM) of Pu in the Np MOPS and $NaHCO_3$ experiments. This Pu trace in the NpO_2^+ stock solution (15 mM HCl) did not have a defined oxidation state speciation. PHREEQC [40] calculations were performed using the specific interaction theory database (sit.dat) [22] to evaluate the equilibria between different aqueous and solid (redox) species of Fe, U, Np and Pu at concentrations relevant to the experimental systems.

2.1. Grazing incidence X-ray Absorption Spectroscopy (GI-XAS).

Single magnetite crystals from the 14 days equilibrated U and Np experiments were analysed for fluorescence detected GI-XAS [41] on the uranium and neptunium L_{III}-edges to determine the speciation of uranium and neptunium on the magnetite surfaces. These analyses were performed at beamline I18 at Diamond Light Source, UK, using a Si(111) monochromator and a 4-element silicon drift fluorescence detector [42]. The energy of the beam was calibrated using the K-edge spectrum of an yttrium foil. The samples were mounted on an eight-axis sample stage (Newport) and the crystals were aligned by positioning them parallel to the beam direction and attenuating to half of the beam intensity as measured by the ion chamber. Next the crystals were rotated along the axis perpendicular to the beam direction to optimise the total external reflection and maximise the intensity of the uranium and neptunium Lα1 fluorescence lines. To minimize the potential of beam induced changes to the magnetite (111) surface (e.g., drying and subsequent decrease in the intensity of the detected fluorescence), the crystals were moved horizontally and realigned during analyses. The uranium and neptunium X-ray absorption spectra collected were inspected for Bragg peaks, merged, normalized and background subtracted using Athena [43]. Athena was also used to determine potential changes in the XANES spectra during the analyses, and confirmed no beam induced damage occurred during the XAS analyses. FEFF8 [44] was used to calculate theoretical scattering paths using the crystallographic information for schoepite [45], magnetite [46] and NpO_2 [47] and the Fourier Transform (in R-space) of the EXAFS spectra were fitted using Artemis [43]; the amplitude correction factor (S_0^2) was fixed at 1 throughout and the statistical validity of the addition of each scattering path was tested using the F-test [48].

2.2. X-ray Photoemission Spectroscopy (XPS).

In addition to the GI-XAS analyses we performed additional analyses using X-ray photoemission spectroscopy (XPS) to provide further insight into the actinide oxidation state in the reacted samples [31,49–51]. The magnetite crystals that were analysed using GI-XAS were returned

to the labs and stored anaerobically at room temperature prior to XPS analysis (SPECS Near-Ambient Pressure XPS system); the XPS analyses were performed at 25 mbar. This allowed us to obtain higher resolution XPS data on the redox speciation of Fe, U, Np (and Pu) on the surface of the equilibrated magnetite crystals. As discussed earlier, trace (ppb) levels of Pu were also present in the Np(V) stock solution and interestingly, these were also detected in the XPS analyses. For the XPS analyses, monochromatic Al Kα X-rays (1486.6 eV) were used. Wide scans were recorded with an analyser pass energy of 60 eV and a step size of 0.5 eV. Narrow scans were recorded with an analyser pass energy of 30 eV and a step size of 0.1 eV. The XPS spectra were processed and analysed using the CasaXPS software package (Casa Software Ltd., UK). The photoelectron binding energies were calibrated by setting the C 1s adventitious carbon peak to 284.8 eV [52]. A Shirley background was used for spectra with high signal to noise ratio, otherwise, a linear background was used. The Fe 2p 3/2 transition was analysed for the Fe(II) and Fe(III) contributions using the methodology described by Biesinger et al. [53]. For the fits to the Fe 2p 3/2 transitions a symmetrical Gaussian Lorentzian peak shape (GL(30)) was used and to minimize the number of independent variables, the relative peak positions and full width half maximum of all peaks were constrained. Furthermore, the relative peak intensities of all Fe(II) peaks were constrained as were all the relative peak intensities for all Fe(III) peaks to the relative peak intensities determined by Biesinger et al. [53]. The analyses of the actinide 4f transitions were based on the methodology described by Ilton et al. [32,51]. The primary peaks for the uranium, neptunium and plutonium 4f transitions were fitted using an asymmetric Gaussian/Lorentzian peak shape (uranium: A(0.35,0.5,0)GL(45), neptunium and plutonium: A(0.25,0.3,0)GL(45)). Any satellite peaks were fitted using a symmetrical Gaussian peak shape (GL(0)). The doublet separation between the actinide 4f 7/2 and 5/2 transitions was kept constant at 10.85, 11.8 and 12.875 eV for uranium, neptunium and plutonium, respectively [54–57] and the ratio of the peak area of the 4f 7/2 and 5/2 transitions was fixed at 0.714 [54–57].

3. Results and Discussion

Figure 1 shows the percentage of uranium and neptunium removed from solution in the MOPS and $NaHCO_3$ buffered experiments. Without carbonate present in solution, U(VI) was almost completely removed from solution after 14 days (99%, U MOPS) while when carbonate was present in solution only ~7% of the added U(VI) was removed from solution after 14 days (U $NaHCO_3$). PHREEQC modelling using the specific ion interaction theory database [22, and references therein] predicts that U(VI) exists dominantly as positively charged polynuclear uranyl hydroxide complexes (72%: $(UO_2)_3(OH)_5^+$, and 22%: $(UO_2)_4(OH)_7^+$) during the U MOPS experiment and dominantly as negatively charged uranyl carbonate complexes (51%: $UO_2(CO_3)_2^{2-}$, 34%: $UO_2(CO_3)_3^{4-}$, and 10%: $(UO_2)_2(CO_3)(OH)_3^-$) during the U $NaHCO_3$ experiment (Table S1). Previous studies have shown that uranyl carbonate species inhibit reduction to U(IV) by decreasing the concentration of aqueous UO_2^{2+} [58]. Furthermore, at pH 7, the interaction of the negatively charged uranyl carbonate species with negatively charged surfaces is also expected to be inhibited [35]. Indeed, it is likely that the inhibition of adsorption and reduction due to the presence of uranyl carbonate complexes also occur on the (111) magnetite surface in the presence of carbonate [59].

In both the Np MOPS and $NaHCO_3$ experiments approximately 28% of the added Np(V) spike activity was removed after 14 days of reaction. PHREEQC using the specific ion interaction theory database [22, and references therein] was used to model the Np(V) speciation in both buffer solutions. Np(V) speciation was predicted to consist of 100% NpO_2^+ in the Np MOPS experiment and of 86% NpO_2^+ and 14% $NpO_2CO_3^-$ in the carbonate experiment. Interestingly, the predicted presence of a significant but not dominant contribution from the negatively charged Np(V) carbonate species did not significantly influence the removal of Np(V) from solution (Figure 1).

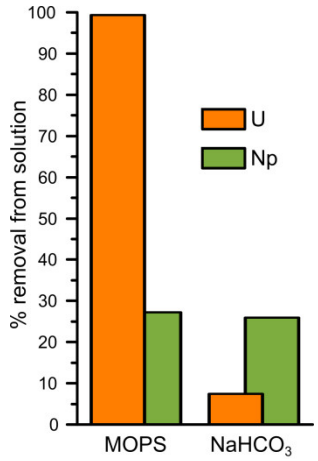

Figure 1. The percentage of removal of uranium and neptunium from solution during the MOPS and $NaHCO_3$ experiments after two weeks of reaction with magnetite.

3.1. Uranium Interaction with Magnetite

The U L_{III}-edge GI-XAS (a-c) and the Fe 2p and U 4f XPS (d and e) results from the magnetite crystals equilibrated with the U MOPS and $NaHCO_3$ buffer solutions are summarised in Figure 2. The XANES spectra from the magnetite crystals equilibrated with both the U MOPS and $NaHCO_3$ buffer solutions were similar to the U(VI) standard rather than the U(IV) standard. This suggests that the uranium speciation on the magnetite crystals was dominated by U(VI) even though magnetite has previously been shown to be able to reduce U(VI) to U(IV).[12,33] Furthermore, the best fits to the EXAFS analyses (Figure 2b,c, and Table 1) include 2 oxygen backscatterers at 1.77 – 1.79Å (reducing the number of oxygen backscatters resulted in an increase in the R-factor) diagnostic for uranyl speciation. Additionally, the fit to the EXAFS from the magnetite crystal equilibrated with the U $NaHCO_3$ buffer solutions included 5 oxygen backscatterers at 2.31 Å and the fit to the EXAFS from the magnetite crystal equilibrated with the U MOPS buffer solution included 6 oxygen backscatterers at 2.21 and 2.41 Å. The best fit to the U MOPS equilibrated magnetite crystal could also be fitted with 0.5 Fe backscatters at 3.49 Å. This suggests that U(VI) interaction with the magnetite (111) surface occurred through the formation of an inner sphere complex as predicted by Missana et al. [60] for uranyl adsorption onto magnetite, and observed in iron oxides, for example, for uranyl adsorption to ferrihydrite [20]. The data quality of the spectrum from the magnetite crystal equilibrated with the U $NaHCO_3$ buffer did not allow detailed interpretation of the species on the surface of magnetite. As observed for the interaction of uranyl with sheet silicates in the presence of carbonate [35] and ferrihydrite [20] this is likely a ternary uranyl-carbonate surface complex, which corresponds with the aqueous speciation of uranyl which is dominated by uranyl carbonate species (Table S1). Overall, the XANES and EXAFS results indicate that uranium removal from solution occurred predominantly through surface complexation of uranyl (U(VI)) species to the magnetite surface.

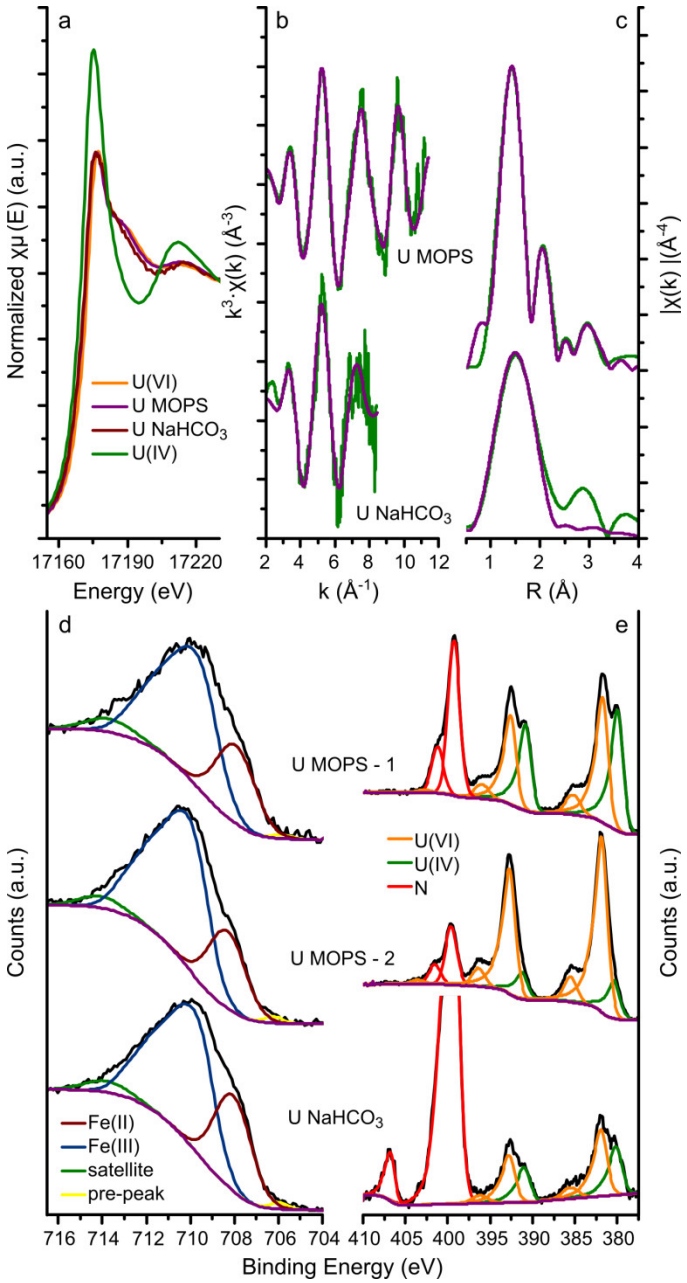

Figure 2. Uranium LIII-edge GI-XAS and the XPS data. Uranium LIII-edge GI-XAS results: **(a)** XANES with U(IV) and U(VI) in-house standards; and **(b and c)** the EXAFS (green lines) and corresponding fits (purple lines) to the U MOPS and U NaHCO3 samples; XPS data for the iron 2p 3/2 transition **(d)** and the uranium 4f 7/2 and 5/2 transitions **(e)** (black lines) and the fits (coloured lines, blue and purple lines represent Fe(III) and Fe(II), respectively, and the orange and green lines represent U(VI) and U(IV), respectively) to the spectra of the U MOPS and U NaHCO3 samples, in the iron 2p 3/2 plot **(d and e)**, the fitted Fe(II) and Fe(III) peaks have been merged for clarity; the U MOPS sample was analysed for XPS on two locations, denoted by – 1 and – 2.

Table 1. Summary of the fits to the uranium and neptunium L_{III}-edge EXAFS for spectra in (Figure 2b,c) U MOPS and U $NaHCO_3$ and Np MOPS and Np $NaHCO_3$ (Figure 3b,c) (CN: coordination number, R: radial distance, σ^2: Debye-Waller factor and S_0^2: amplitude correction factor, MS: multiple scattering); included is also the size of the XANES edge step before normalization (Figure 2a and 3a).

Sample	Scattering Path	CN	R (Å)	σ^2 (Å^2)	S_0^2	R-factor
U MOPS[1]	U-O_{ax}	2[2]	1.788(4)	0.0045(5)	1[2]	0.007
Edge step: 1.7	U-O_{eq}	3[2]	2.205(7)	0.0051(9)		
	U-O_{eq}	3[2]	2.408(8)	0.0035(9)		
	U-Fe	0.5[2]	3.49(3)	0.006(3)		
	U-O_{ax} (MS)	6[2]	3.575[2]	0.0089[2]		
U $NaHCO_3$	U-O_{ax}	2[2]	1.80(7)	0.010(8)	1[2]	0.01
Edge step: 0.039	U-O_{eq}	5[2]	2.35(13)	0.014(11)		
Np MOPS	Np-O	8[2]	2.34(4)	0.009(2)	1[2]	0.03
Edge step: 0.013						
Np $NaHCO_3$	Np-O	8[2]	2.32(3)	0.011(2)	1[2]	0.03
Edge step: 0.018						

[1] All added scattering paths have a confidence level > 90%, calculated using the F-test for EXAFS [48];
[2] Fixed or constrained values.

The XPS data and their respective fits are summarized in Figure 2d,e and Table 2 and S2. The fits to the Fe 2p 3/2 transition are representative of magnetite and fitting using the methodology by Biesinger et al. [53], resulted in calculation of the relative amounts of Fe(II) and Fe(III) in magnetite assuming the area under the fitted peaks is linearly proportional to the respective fraction of Fe. Table 2 shows that the Fe(II) contribution to the 2p 3/2 transition varied from 23.6% to 29.4%, compared to a predicted Fe(II) contribution of 33.3% in stoichiometric magnetite. This shows that the magnetite crystals were (slightly) sub-stoichiometric and suggesting partial oxidation of the surface. A variation in the contribution of Fe(II) to the 2p 3/2 transition was also observed for two different spots on the same crystal (U MOPS-1: 23.6% and U MOPS-2: 26.5%). The (polished) crystals were prepared from natural magnetite samples and used as received, hence, we postulate that this variation resulted either from variations in the ratio of octahedrally and tetrahedrally coordinated iron on the surface,[61] or from variations in magnetite oxidation to maghemite (i.e., variations in a magnetite-maghemite solid solution) at the surfaces of such a natural sample [29,30].

Table 2. Summary of the fits to the XPS results from the U (Figure 2d,e) and the Np (Figure 3d,e) samples; the values represent the percentages of the fitted areas of the peaks associated with the different redox states of Fe, U, Pu and Np; the U MOPS sample was analysed on two locations, denoted by –1 and –2.

	Fe(II)	Fe(III)	Pre-peak	Satellite (Fe(III))	U(IV)	U(VI)	Pu(III)	Pu(IV)	Np(IV)
U MOPS-1	26.5	67.3	0.7	5.5	43.8	56.2	-	-	-
U MOPS-2	23.6	71.2	1.0	4.2	15.5	84.5	-	-	-
U $NaHCO_3$	29.4	65.5	1.0	4.1	37.5	62.5	-	-	-
Np/Pu MOPS	27.5	66.5	1.0	5.0	-	-	65.6	34.4	100
Np/Pu $NaHCO_3$	26.9	67.6	0.9	4.6	-	-	53.0	47.0	100

The uranium 4f 7/2 and 5/2 transitions were fitted to obtain more detailed information on the uranium oxidation state (Figure 2a-c and Table 1) [49]. Here, the peaks of the uranium 4f 7/2 and 5/2 transitions were best fitted with two U species only: U(VI) and U(IV). The binding energy of the 4f 7/2 transition for these two species was fitted to be 380.2–380.7 eV and 381.6–382.2 eV (Table S2), with peak separations (ΔE) observed at 1.3–1.8 eV. These binding energies are within the range determined for U(IV) and U(VI) [27,32,51,55,59,62,63]. Additionally, the observed peak separations (1.3-1.8 eV) are larger than expected for a system with U(V) present (observed ΔE of the U 4f 7/2 transitions for U(V) and U(VI) is 0.8–1.0 eV; ΔE for U(IV) and U(VI) is 1.3–1.5 eV) confirming our interpretation that

the dominant species are U(VI) and U(IV) [52]. The observation of U(IV) on the magnetite (111) using XPS compared to the lack of any observable U(IV) contribution to the EXAFS spectra may be the result of heterogeneity, with the XPS analyses probing a much smaller area than the GI-XAS analyses. Also there are often challenges associated in determining the uranium oxidation state using conventional XAS techniques [49]. For example, possible preferred orientation of the uranyl moiety on the magnetite surface combined with a (polarized) synchrotron X-ray beam could result in an overestimation of the U-O_{ax} coordination number based on the EXAFS analyses [41]. The two techniques should be probing roughly the same depth. Singer et al. determined that on stoichiometric magnetite (111) surfaces (Fe(II): 33.3%), the U(IV) accounts for 41–42% and 35–36% in the absence and presence of bicarbonate respectively [27]. This is comparable to the presented results for U MOPS-1 (Fe(II): 26.5%; U(IV): 43.8%) and U $NaHCO_3$ (Fe(II): 29.4%; U(IV): 37.5%) (Table 2). On the other hand, the location on the magnetite crystal equilibrated with the U MOPS buffer solutions with the lowest fitted Fe(II) contribution to the Fe 2p 3/2 transition (Fe(II) = 23.6%) shows a U(IV) contribution to the uranium 4f 7/2 and 5/2 transitions (15.5% U(IV)) significantly lower than that expected for stoichiometric magnetite and observed for U MOPS-1. These trends agree with past observations that lower Fe(II)/(III) ratios at the surface of magnetite [23] and increased HCO_3^- concentrations reduce the potential for U(VI) reduction to U(IV) on the (111) surface of magnetite [27]. Interestingly, no U(V) contribution to the U 4f 7/2 and 5/2 transitions could be fitted on these single crystal magnetite experiments, and in contrast to nanoparticulate magnetite systems where U(V) was observed [32,34].

The iron and uranium redox couples were further examined using PHREEQC modelling in the presence of MOPS and HCO_3^- buffers and summarized in Figure S1. This shows that U(VI) reduction to U(IV) as uraninite (crystalline UO_2) coupled to iron oxidation is thermodynamically favourable (Figure S1). However, in natural systems reduction of U(VI) to U(IV) generally favours the formation of nanocrystalline uraninite with a reported stability similar to amorphous UO_2 phases [27,35]. PHREEQC modelling suggests that the reduction of U(VI) to amorphous UO_2 coupled with Fe(II) oxidation to Fe(III) is thermodynamically unfavourable (Figure S1). This could explain the limited amount uranium reduction on the magnetite surface (Figure 2a–c). Finally, the XPS data (Figure 2d–e) highlight the influence of the surface Fe(II) in the magnetite crystal on the extent of U(VI) reduction consistent with the observations of Latta et al. [23].

3.2. Neptunium (and Plutonium) Interactions with Magnetite

Figure 3 summarizes the Np L_{III}-edge GI-XAS data (a-c), the Fe 2p, Np and Pu 4f XPS data (d) and the UV-Vis spectroscopy data (f) from the Np MOPS and $NaHCO_3$ experiments. We also note the presence of Pu in the XPS data resulting from an impurity in the Np stock. This nano molar Pu concentration gave an XPS signal which we were able to fit (Figure 3e).

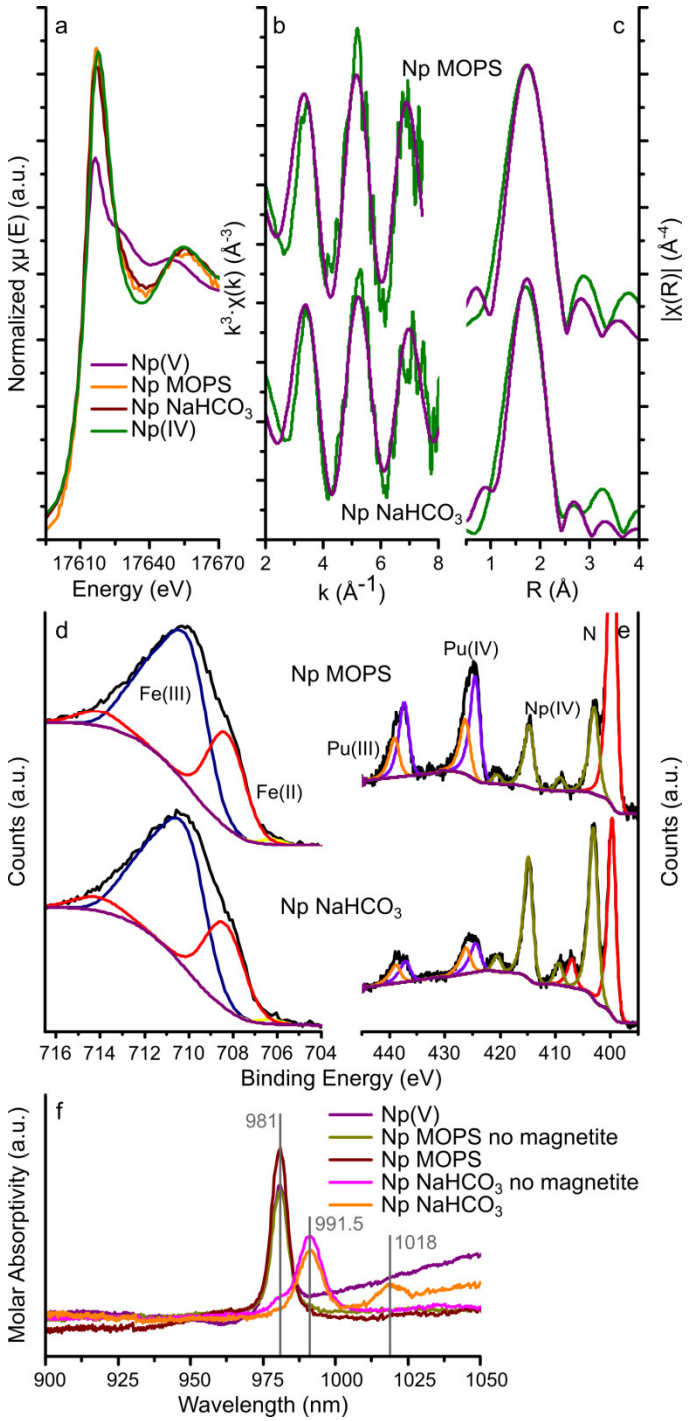

Figure 3. Neptunium L_{III}-edge GI-XAS, XPS, and UV-Vis spectroscopy data. Neptunium L_{III}-edge XAS results: **(a)** XANES with aqueous Np(IV) and Np(V) standards [64]; and **(b and c)** EXAFS (green lines) and corresponding fits (purple lines) to the Np MOPS and Np $NaHCO_3$ samples; XPS data for the iron 2p 3/2 transition **(d)**, and neptunium (and plutonium) 4f 7/2 and 5/2 transitions **(e)** (black lines) and fits to the spectra (coloured lines, blue and purple lines represent Fe(III) and Fe(II), respectively, the purple and orange lines represent Pu(IV) and Pu(III), respectively, and the olive lines represent Np(IV) for the Np MOPS and Np $NaHCO_3$ samples, in the iron 2p 3/2 plot **(d)**, in the iron 2p 3/2 plot **(d)**, the fitted Fe(II) and Fe(III) peaks have been merged for clarity; and **(f)** the UV-Vis spectra for a pH 4 NpO_2^+ (Np(V)) solution (prepared by diluting the stock solution in DI water only), two solutions with 10 ppm neptunium and 10 mM MOPS (Np MOPS no magnetite) or 5 mM $NaHCO_3$ (Np $NaHCO_3$ no magnetite) and the aqueous phase after 14 days equilibration with magnetite (Np MOPS and Np $NaHCO_3$), the vertical grey lines represent the absorption bands observed in the spectra.

3.2.1. Neptunium

The XANES spectra from the magnetite crystals equilibrated with the Np MOPS and $NaHCO_3$ buffers had similar edge steps (0.013 and 0.018, respectively, Table 1) suggesting that the magnitude of neptunium interaction with the magnetite (111) surfaces was similar. This confirms the aqueous geochemistry data where removal was approximately 28% from both buffer solutions (Figure 1). Additionally, the shape of the XANES from these two samples was comparable and very similar to the Np(IV) standard (Figure 3a) indicating that the oxidation state of neptunium on the magnetite (111) surface was dominated by Np(IV). Fitting the Np L_{III}-edge EXAFS spectra from the magnetite crystals equilibrated with the Np MOPS and Np $NaHCO_3$ buffer solutions was possible with a single shell of 8 oxygen backscatterers at 2.32–2.34 Å (Figure 3b and c and Table 1). No statistical validity could be achieved by adding Np(V)-O_{ax} scattering paths at 1.8–1.9 Å confirming no significant dioxygenyl Np(V) (NpO_2^+) was present on the magnetite crystals. Additionally, due to the data quality of the EXAFS spectra, no further backscatterers (Np or Fe) could be fit to the spectra and thus it was not possible to distinguish between nanoparticulate NpO_2 or surface bound Np^{4+} [16,35,38,65].

The fits to the neptunium 4f 7/2 and 5/2 transitions of the XPS spectra from both magnetite crystals (Figure 3e) could be modelled as a single Np(IV) species with binding energies for the neptunium 4f 7/2 and 5/2 transitions of 403.2–403.4 and 415.0–415.2 eV (Table S2), respectively. These binding energies and the presence of satellite peaks for the neptunium 4f transitions match previously determined binding energies for Np(IV) (4f 7/2: 402.8-403.8 eV and 4f 5/2: 414.3-414.6 eV) [54,56,66–68] and further confirm Np(IV) as the dominant redox state of neptunium as observed from the GI-XAS analyses. Furthermore, the fits to the Fe 2p 3/2 transition are representative of magnetite and fitting using the methodology by Biesinger et al. [53] resulted in relative amounts of Fe(II) and Fe(III) in magnetite assuming the area under the fitted peaks is linearly proportional to the respective fraction of Fe. Table 2 shows that the Fe(II) contribution to the 2p 3/2 transition of 27.5% and 26.9% for the magnetite crystal equilibrated with the Np MOPS and Np $NaHCO_3$ buffer solutions, respectively, compared to a predicted Fe(II) contribution of 33.3% in stoichiometric magnetite. This suggests (slightly) sub-stoichiometric magnetite similar to the U experiments.

The results from the UV-Vis spectroscopy on the aqueous phase before and after equilibration with magnetite are plotted in Figure 3f and include the spectra of a Np(V) standard solution at pH 4 (0.1mM HCl), the Np MOPS and Np $NaHCO_3$ buffer solutions equilibrated with the magnetite single crystals and parallel Np MOPS and Np $NaHCO_3$ controls which were not equilibrated with the magnetite single crystals. The UV-Vis spectrum of the pH 4 Np(V) solution exhibits a single, intense absorption band at 981 nm, consistent with NpO_2^+ [69] and confirming the oxidation state of Np(V) in the stock solution. The UV-Vis spectra of both of the Np MOPS buffer solutions (with and without magnetite) also show this single absorption band at 981 nm confirming NpO_2^+ dominated in solution even after reaction with the magnetite crystal. The spectra of the Np $NaHCO_3$ buffer not equilibrated with magnetite shows a dominant absorption band at 991.5 nm and a shoulder at 981 nm (Figure 3f), indicative of both $NpO_2CO_3^-$ and (less) NpO_2^+ [69]. Interestingly, the UV-Vis spectrum for the Np $NaHCO_3$ buffer equilibrated with magnetite does not exhibit the NpO_2^+ absorption band at 981 nm, rather an absorption band is observed at 1018 nm in addition to the $NpO_2CO_3^-$ absorption band at 991.5 nm (Figure 3f). To the best of our knowledge, an absorption band at 1018 nm for neptunium has not been observed, to date. The absorption band at 1018 nm is absent in the UV-Vis spectra for the solutions not reacted with magnetite (Figure 3f). This suggests that this absorption band could be a result of NpO_2^+ complexing with, both, CO_3^{2-} and Fe(II) or Fe(III). The identification of such a potential ternary complex warrants further investigation but it appears to be similar to ternary complexes of hexavalent uranyl with carbonate and alkaline earth metals [70] and the postulated ternary complex of pentavalent uranyl with carbonate and iron [71].

Interestingly, the differences in the aqueous speciation of neptunyl observed in the UV-vis spectra did not affect the removal of Np from solution during the interaction with the magnetite crystals (Figure 1). Finally, the UV-Vis spectra indicate that Np in solution is dominated by Np(V), and the GI-XAS and XPS data confirm that Np on the magnetite (111) surface after two weeks is dominated by Np(IV). Combined with the dominance of Np(V) species in solution in both buffer

solutions, this indicates that reduction of Np(V) on magnetite appears surface mediated [16,28], regardless of the presence or absence of aqueous bicarbonate.

3.2.2. Plutonium

The XPS of the Np MOPS and $NaHCO_3$ samples also show clear peaks representing the Pu 4f 7/2 and 5/2 transitions at similar intensities to the Np 4f 7/2 and 5/2 transitions (Figure 3e). Taking into account that the experimental solutions contained in the order of 0.1% Pu by mass (compared to Np), this indicates that that the interaction of Pu with magnetite is significantly stronger than that of Np(V). Furthermore, the plutonium 4f 7/2 and 5/2 transitions could be fit with two species (Figure 3e), with binding energies of 424.8–424.9 eV and 426.5–426.6 eV for the 4f 7/2 transitions and 437.6–437.7 eV and 439.3–439.4 eV for the 4f 5/2 transitions (Table S2). These binding energies correspond very well to previously reported binding energies for Pu(III) (4f 7/2: 424.4 eV; 4f 5/2: 437.2–437.6 eV) and Pu(IV) (4f 7/2: 425.8–427.0 eV; 4f 5/2: 438.5–439.3 eV) [54,57,66,68,72,73] (Table 2). The observation of Pu(III) and Pu(IV) on the surface of the magnetite crystals is compatible with previous observations of either Pu(III) or Pu(IV) on the surface of magnetite [13,17], while more focused experimental investigations are essential to determine the influence of HCO_3^- on the surface reactivity and speciation of Pu(IV) and Pu(III), including their respective aqueous speciation (Table S1).

4. Conclusions

Here we show that uranium (as UO_2^{2+} complexes) interacts with magnetite surfaces through surface complexation of uranyl and partial reduction to U(IV). The surface complexation of UO_2^{2+} is highly dependent on the presence of bicarbonate in solution through the formation of negatively charged aqueous uranyl carbonate complexes. By complementing GI-XAS with XPS analyses, we show that uranium speciation on magnetite crystals is dominated by U(VI) surface complexes (GI-XAS) and that the extent of uranium reduction is variable on a single magnetite crystal and dependent on the stoichiometry of magnetite (XPS). Also, there was no evidence for pentavalent uranium in these reactions with a (111) crystal face of magnetite and in contrast to interactions with nanoparticulate magnetite or during the formation of nanoparticulate magnetite. For neptunium, and combining GI-XAS, XPS and UV-Vis spectroscopy, we determined that the interaction of neptunium (as NpO_2^+) is independent of the presence of carbonate in solution and resulting aqueous complexes, with 28% of Np removed from solution in in the presence and absence of carbonate, and exhibited a dominant oxidation state of Np(IV) on the magnetite crystals. Even though the extent of interaction between Np(V) and the magnetite (111) surface did not vary depending on the presence of bicarbonate, the aqueous Np speciation (as detected by UV-Vis spectroscopy) was significantly different, with 100% of the Np(V) present as NpO_2^+ in the absence of carbonate. The aqueous speciation, in the presence of carbonate was dominated by $NpO_2CO_3^-$, while after the interaction with magnetite we suggest a previously unidentified aqueous species appeared as identified by the appearance of an absorption band at 1018 nm in the UV-Vis spectra. Based on the aqueous chemistry of the experiments, we propose that this is likely a ternary Np(V) complex with (bi)carbonate and iron. Finally, XPS analyses showed Pu, from impurities in the Np stock, was strongly associated with the magnetite crystals and displayed both Pu(III) and Pu(IV) oxidation states. Overall, the presented results highlight the differences between uranium, neptunium and plutonium interaction with magnetite, and reaffirm the importance of bicarbonate present in the aqueous phase.

Supplementary Materials: The following are available online at www.mdpi.com/xxx/s1, Figure S1: stability fields for the dominant redox species for Fe, U, Np and Pu based on geochemical speciation modeling using PHREEQC, Table S1: dominant aqueous speciation of U, Np and Pu based on the geochemical speciation modelling using PHREEQC, Table S2: summary of the binding energies (XPS) of the main peaks for the actinide 4f transitions.

Author Contributions: P.B., A.V.V., R.A.W. and K.M. conceived and designed the experiments; P.B. and A.V.V. performed the experiments, P.B., A.V.V., J.F.W.M., R.A.W., and K.M. performed the GI-

XAS analyses and P.B., J.F.W.M. and K.M. interpreted the GI-XAS results; P.B. and C.M. performed the XPS analyses and interpreted the results; P.B. wrote the manuscript and A.V.V., J.F.W.M., C.M., R.A.W. and K.M. participated in revising the manuscript.

Funding: This research was funded by the EPSRC grant: "Atomic and Macro-scale Studies of Surface Processes: Towards a Mechanistic Understanding of Surface Reactivity and Radionuclide Binding Mechanisms" [EP/I036389/1] and the GI-XAS analyses were funded by Diamond Light Source [SP11412].

Acknowledgments: We would like to thank Paul Lythgoe for the ICP-MS analyses of the uranium samples Richard Doull for radiological safety advice and assistance at Diamond Light Source and Daisy Ray and Gareth Law for performing the α-spectroscopy analysis on the ^{237}Np stock solution.

Conflicts of Interest: The authors declare no conflict of interest.

References

1. Morris, K.; Law, G.T.W.; Bryan, N.D. Geodisposal of Higher Activity Wastes. In *Nuclear Power and the Environment*; The Royal Society of Chemistry: London, UK, 2011; pp. 129–151. doi:10.1039/9781849732888-00129
2. Cantrell, K.J.; Um, W.; Williams, B.D.; Bowden, M.E.; Gartman, B.; Lukens, W.W.; Buck, E.C.; Mausolf, E.J. Chemical stabilization of Hanford tank residual waste. *J. Nucl. Mater.* **2014**, *446*, 246–256. doi:10.1016/j.jnucmat.2013.10.060
3. Cendón, D.I.; Hughes, C.E.; Harrison, J.J.; Hankin, S.I.; Johansen, M.P.; Payne, T.E.; Wong, H.; Rowling, B.; Vine, M.; Wilsher, K.; et al. Identification of sources and processes in a low-level radioactive waste site adjacent to landfills: Groundwater hydrogeochemistry and isotopes. *Aust. J. Earth Sci.* **2015**, *62*, 123–141, doi:10.1080/08120099.2015.975155.
4. Payne, T.E.; Harrison, J.J.; Hughes, C.E.; Johansen, M.P.; Thiruvoth, S.; Wilsher, K.L.; Cendón, D.I.; Hankin, S.I.; Rowling, B.; Zawadzki, A. Trench 'Bathtubbing' and surface plutonium contamination at a legacy radioactive waste site. *Environ. Sci. Technol*. **2013**, *47*, 13284–13293, doi:10.1021/es403278r.
5. Anderson, R.T.; Vrionis, H.A.; Ortiz-Bernad, I.; Resch, C.T.; Long, P.E.; Dayvault, R.; Karp, K.; Marutzky, S.; Metzler, D.R.; Peacock, A.; et al. Stimulating the in situ activity of Geobacter species to remove uranium from the groundwater of a uranium-contaminated aquifer. *Appl. Environ. Microbiol.* **2003**, *69*, 5884–5891, doi:10.1128/aem.69.10.5884-5891.2003.
6. Suzuki, Y.; Kelly, S.D.; Kemner, K.M.; Banfield, J.F. Microbial populations stimulated for hexavalent uranium reduction in uranium mine sediment. *Appl. Environ. Microbiol.* **2003**, *69*, 1337–1346, doi:10.1128/AEM.69.3.1337-1346.2003.
7. Law, G.T.W.; Geissler, A.; Burke, I.T.; Livens, F.R.; Lloyd, J.R.; McBeth, J.M.; Morris, K. Uranium redox cycling in sediment and biomineral systems. *Geomicrobiol. J.* **2011**, *28*, 497–506, doi:10.1080/01490451.2010.512033.
8. Marsdem, O.J.; Abrahamsen, L.; Brayan, N.D.; Day Philip, J.; Fifield, K.; Gent, C.; Goodal, P.S.; Morris, K.; Livens, F.R. Transport and accumulation of actinide elements in the near-shore environment: Field and modelling studies. *Sedimentology* **2006**, *53*, 237–248, doi:10.1111/j.1365-3091.2005.00761.x.
9. Duro, L.; Domènech, C.; Grivé, M.; Roman-Ross, G.; Bruno, J.; Källström, K. Assessment of the evolution of the redox conditions in a low and intermediate level nuclear waste repository (SFR1, Sweden). *Appl. Geochem.* **2014**, *49*, 192–205, doi:10.1016/j.apgeochem.2014.04.015.
10. Bots, P.; Shaw, S.; Law, G.T.W.; Marshall, T.A.; Mosselmans, J.F.W.; Morris, K. Controls on the Fate and Speciation of Np(V) during Iron (Oxyhydr)oxide Crystallization. *Environ. Sci. Technol.* **2016**, *50*, 3382–3390, doi:10.1021/acs.est.5b05571.
11. Marshall, T.A.; Morris, K.; Law, G.T.W.; Livens, F.R.; Mosselmans, J.F.W.; Bots, P.; Shaw, S. Incorporation of uranium into hematite during crystallization from ferrihydrite. *Environ. Sci. Technol.* **2014**, *48*, 3724–3731, doi:10.1021/es500212a.
12. Marshall, T.A.; Morris, K.; Law, G.T.W.; Mosselmans, F.W.; Bots, P.; Roberts, H.; Shaw, S. Uranium fate during crystallization of magnetite from ferrihydrite in conditions relevant to the disposal of radioactive waste. *Miner. Mag.* **2015**, *79*, 1265–1274, doi:10.1180/minmag.2015.079.6.02.

13. Powell, B.A.; Fjeld, R.A.; Kaplan, D.I.; Coates, J.T.; Serkiz, S.M. Pu(V)O2+ Adsorption and Reduction by Synthetic Magnetite (Fe3O4). *Environ. Sci. Technol.* **2004**, *38*, 6016–6024, doi:10.1021/es049386u.
14. Tinnacher, R.M.; Zavarin, M.; Powell, B.A.; Kersting, A.B. Kinetics of neptunium(V) sorption and desorption on goethite: An experimental and modeling study. *Geochim. Cosmochim. Acta* **2011**, *75*, 6584–6599, doi:10.1016/j.gca.2011.08.014.
15. Wong, J.C.; Zavarin, M.; Begg, J.D.; Kersting, A.B.; Powell, B.A. Effect of equilibration time on Pu desorption from goethite. *Radiochim. Acta* **2015**, *103*, 695–705, doi:10.1515/ract-2015-2404.
16. Wylie, E.M.; Olive, D.T.; Powell, B.A. Effects of Titanium Doping in Titanomagnetite on Neptunium Sorption and Speciation. *Environ. Sci. Technol.* **2016**, *50*, 1853–1858, doi:10.1021/acs.est.5b05339.
17. Kirsch, R.; Fellhauer, D.; Altmaier, M.; Neck, V.; Rossberg, A.; Fanghänel, T.; Charlet, L.; Scheinost, A.C. Oxidation state and local structure of plutonium reacted with magnetite, mackinawite, and chukanovite. *Environ. Sci. Technol.* **2011**, *45*, 7267–7274, doi:10.1021/es200645a.
18. Pidchenko, I.; Heberling, F.; Kvashnina, K.O.; Finck, N.; Schild, D.; Bohnert, E.; Schäfer, T.; Rothe, J.; Geckeis, H.; Vitova, T. Aqueous U(VI) interaction with magnetite nanoparticles in a mixed flow reactor system: HR-XANES study. *J. Phys. Conf. Ser.* **2016**, *712*, 012086. doi:10.1088/1742-6596/712/1/012086
19. Li, D.; Kaplan, D.I. Sorption coefficients and molecular mechanisms of Pu, U, Np, Am and Tc to Fe (hydr)oxides: A review. *J. Hazard. Mater.* **2012**, *243*, 1–18, doi:10.1016/j.jhazmat.2012.09.011.
20. Waite, T.D.; Davis, J.A.; Payne, T.E.; Waychunas, G.A.; Xu, N. Uranium(VI) adsorption to ferrihydrite: Application of a surface complexation model. *Geochim. Cosmochim. Acta* **1994**, *58*, 5465–5478, doi:10.1016/0016-7037(94)90243-7.
21. Roberts, H.E.; Morris, K.; Law, G.T.W.; Mosselmans, J.F.W.; Bots, P.; Kvashnina, K.; Shaw, S. Uranium(V) Incorporation Mechanisms and Stability in Fe(II)/Fe(III) (oxyhydr)Oxides. *Environ. Sci. Technol. Letters* **2017**, *4*, 421–426, doi:10.1021/acs.estlett.7b00348.
22. Guillaumont, R.; Fanghänel, T.; Neck, V.; Guger, J.; Palmer, D.A.; Grenthe, I.; Rand, M.H. *Update on the Chemical Thermodynamics of Uranium, Neptunium, Plutonium, Americium and Technetium*; OECD Nuclear Energy Agency, Data Bank: Issy-les-Moulineaux, France, 2003.
23. Latta, D.E.; Gorski, C.A.; Boyanov, M.I.; O'Loughlin, E.J.; Kemner, K.M.; Scherer, M.M. Influence of magnetite stoichiometry on U VI reduction. *Environ. Sci. Technol.* **2012**, *46*, 778–786, doi:10.1021/es2024912.
24. Latta, D.E.; Mishra, B.; Cook, R.E.; Kemner, K.M.; Boyanov, M.I. Stable U(IV) Complexes Form at High-Affinity Mineral Surface Sites. *Environ. Sci. Technol.* **2014**, doi:10.1021/es4047389.
25. Latta, D.E.; Boyanov, M.I.; Kemner, K.M.; O'Loughlin, E.J.; Scherer, M.M. Abiotic reduction of uranium by Fe(II) in soil. *Appl. Geochem.* **2012**, *27*, 1512–1524, doi:10.1016/j.apgeochem.2012.03.003.
26. Scott, T.B.; Allen, G.C.; Heard, P.J.; Randell, M.G. Reduction of U(VI) to U(IV) on the surface of magnetite. *Geochim. Cosmochim. Acta* **2005**, *69*, 5639–5646, doi:10.1016/j.gca.2005.07.003.
27. Singer, D.M.; Chatman, S.M.; Ilton, E.S.; Rosso, K.M.; Banfield, J.F.; Waychunas, G.A. Identification of simultaneous U(VI) sorption complexes and U(IV) nanoprecipitates on the magnetite (111) surface. *Environ. Sci. Technol.* **2012**, *46*, 3811–3820. doi:10.1021/es203877x
28. Nakata, K.; Nagasaki, S.; Tanaka, S.; Sakamoto, Y.; Tanaka, T.; Ogawa, H. Reduction rate of neptunium(V) in heterogeneous solution with magnetite. *Radiochim. Acta* **2004**, *92*, 145–149, doi:10.1524/ract.92.3.145.30493.
29. Tang, J.; Myers, M.; Bosnick, K.A.; Brus, L.E. Magnetite Fe_3O_4 Nanocrystals: Spectroscopic Observation of Aqueous Oxidation Kinetics. *J. Phys. Chem. B* **2003**, *107*, 7501–7506, doi:10.1021/jp027048e.
30. White, A.F.; Peterson, M.L.; Hochella, M.F. Electrochemistry and dissolution kinetics of magnetite and ilmenite. *Geochim. Cosmochim. Acta* **1994**, *58*, 1859–1875, doi:10.1016/0016-7037(94)90420-0.
31. Huber, F.; Schild, D.; Vitova, T.; Rothe, J.; Kirsch, R.; Schäfer, T. U(VI) removal kinetics in presence of synthetic magnetite nanoparticles. *Geochim. Cosmochim. Acta* **2012**, *96*, 154–173. doi:10.1016/j.gca.2012.07.019
32. Ilton, E.S.; Boily, J.F.S.; Buck, E.C.; Skomurski, F.N.; Rosso, K.M.; Cahill, C.L.; Bargar, J.R.; Felmy, A.R. Influence of dynamical conditions on the reduction of UVI at the magnetite-solution interface. *Environ. Sci. Technol.* **2010**, *44*, 170–176, doi:10.1021/es9014597.
33. Missana, T.; Maffiotte, C.; García-Gutiérrez, M. Surface reactions kinetics between nanocrystalline magnetite and uranyl. *J. Colloid Interface Sci.* **2003**, *261*, 154–160, doi:10.1016/S0021-9797(02)00227-8.
34. Yuan, K.; Ilton, E.S.; Antonio, M.R.; Li, Z.; Cook, P.J.; Becker, U. Electrochemical and Spectroscopic Evidence on the One-Electron Reduction of U(VI) to U(V) on Magnetite. *Environ. Sci. Technol.* **2015**, *49*, 6206–6213, doi:10.1021/acs.est.5b00025.

35. Brookshaw, D.R.; Pattrick, R.A.D.; Bots, P.; Law, G.T.W.; Lloyd, J.R.; Mosselmans, J.F.W.; Vaughan, D.J.; Dardenne, K.; Morris, K. Redox interactions of Tc(VII), U(VI) and Np(V) with microbially reduced biotite and chlorite. *Environ. Sci. Technol.* **2015**, *79*, 13139–13148, doi:10.1021/acs.est.5b03463.
36. Begg, J.D.; Zavarin, M.; Zhao, P.; Tumey, S.J.; Powell, B.; Kersting, A.B. Pu(V) and Pu(IV) sorption to montmorillonite. *Environ. Sci. Technol.* **2013**, *47*, 5146–5153, doi:10.1021/es305257s.
37. Zhao, P.; Begg, J.D.; Zavarin, M.; Tumey, S.J.; Williams, R.; Dai, Z.R.; Kips, R.; Kersting, A.B. Plutonium(IV) and (V) Sorption to Goethite at Sub-Femtomolar to Micromolar Concentrations: Redox Transformations and Surface Precipitation. *Environ. Sci. Technol.* **2016**, *50*, 6948–6956, doi:10.1021/acs.est.6b00605.
38. Law, G.T.W.; Geissler, A.; Lloyd, J.R.; Livens, F.R.; Boothman, C.; Begg, J.D.C.; Denecke, M.A.; Rothe, J.; Dardenne, K.; Burke, I.T.; et al. Geomicrobiological Redox Cycling of the Transuranic Element Neptunium. *Environ. Sci. Technol.* **2010**, *44*, 8924–8929, doi:10.1021/es101911v.
39. Singer, D.M.; Chatman, S.M.; Ilton, E.S.; Rosso, K.M.; Banfield, J.F.; Waychunas, G.A. U(VI) Sorption and Reduction Kinetics on the Magnetite (111) Surface. *Environ. Sci. Technol.* **2012**, *46*, 3821–3830, doi:10.1021/es203878c.
40. Parkhurst, D.L.; Appelo, C.A.J. *User's Guide to PHREEQC (Version 2)—A Computer Program for Speciation, Batch-Reaction, One-Dimensional Transport, and Inverse Geochemical Calculations*; U.S. Geological Survey: Denver, CO, USA, 1999; pp. 312. doi:10.3133/wri994259
41. Van Veelen, A.; Bargar, J.R.; Law, G.T.W.; Brown, G.E.; Wogelius, R.A. Uranium Immobilization and Nanofilm Formation on Magnesium-Rich Minerals. *Environ. Sci. Technol.* **2016**, *50*, 3435–3443, doi:10.1021/acs.est.5b06041.
42. Mosselmans, J.F.W.; Quinn, P.D.; Dent, A.J.; Cavill, S.A.; Moreno, S.D.; Peach, A.; Leicester, P.J.; Keylock, S.J.; Gregory, S.R.; Atkinson, K.D.; et al. I18—The microfocus spectroscopy beamline at the Diamond Light Source. *J. Synchrotron Radiat.* **2009**, *16*, 818–824, doi:10.1107/S0909049509032282.
43. Ravel, B.; Newville, M. ATHENA, ARTEMIS, HEPHAESTUS: Data analysis for X-ray absorption spectroscopy using IFEFFIT. *J. Synchrotron Radiat.* **2005**, *12*, 537–541, doi:10.1107/s0909049505012719.
44. Ankudinov, A.L.; Ravel, B.; Rehr, J.J.; Conradson, S.D. Real-space multiple-scattering calculation and interpretation of x-ray-absorption near-edge structure. *Phys. Rev. B* **1998**, *58*, 7565–7576. doi:10.1103/PhysRevB.58.7565
45. Finch, R.J.; Cooper, M.A.; Hawthorne, F.C.; Ewing, R.C. The crystal structure of schoepite,[(UO 2) 8 O 2 (OH) 12](H 2 O) 12. *Can. Mineral.* **1996**, *34*, 1071–1088.
46. Fleet, M. The structure of magnetite. *Acta Crystallogr. Sect. B* **1981**, *37*, 917–920, doi:10.1107/S0567740881004597.
47. Zachariasen, W.H. Crystal chemical studies of the 5f-Series of elements. XII. New compounds representing known structure types. *Acta Crystallogr.* **1949**, *2*, 388–390.
48. Downward, L.; Booth, C.H.; Lukens, W.W.; Bridges, F. A variation of the F-test for determining statistical relevance of particular parameters in EXAFS fits. *AIP Conference Proceedings*. **2006**, *882,* 129–131. doi:10.1063/1.264450.
49. Kvashnina, K.O.; Kvashnin, Y.O.; Butorin, S.M. Role of resonant inelastic X-ray scattering in high-resolution core-level spectroscopy of actinide materials. *J. Electron Spectrosc. Relat. Phenom.* **2014**, *194*, 27–36. doi: 10.1016/j.elspec.2014.01.016
50. Denecke, M.A.; Dardenne, K.; Marquardt, C.M. Np(IV)/Np(V) valence determinations from Np L3 edge XANES/EXAFS. *Talanta* **2005**, *65*, 1008–1014, doi:10.1016/j.talanta.2004.08.034.
51. Ilton, E.S.; Bagus, P.S. XPS determination of uranium oxidation states. *Surf. Interface Anal.* **2011**, *43*, 1549–1560, doi:10.1002/sia.3836.
52. Ilton, E.S.; Boily, J.F.; Bagus, P.S. Beam induced reduction of U(VI) during X-ray photoelectron spectroscopy: The utility of the U4f satellite structure for identifying uranium oxidation states in mixed valence uranium oxides. *Surf. Sci.* **2007**, *601*, 908–916, doi:10.1016/j.susc.2006.11.067.
53. Biesinger, M.C.; Payne, B.P.; Grosvenor, A.P.; Lau, L.W.M.; Gerson, A.R.; Smart, R.S.C. Resolving surface chemical states in XPS analysis of first row transition metals, oxides and hydroxides: Cr, Mn, Fe, Co and Ni. *Appl. Surf. Sci.* **2011**, *257*, 2717–2730, doi:10.1016/j.apsusc.2010.10.051.
54. Veal, B.W.; Lam, D.J.; Diamond, H.; Hoekstra, H.R. X-ray photoelectron-spectroscopy study of oxides of the transuranium elements Np, Pu, Am, Cm, Bk, and Cf. *Phys. Rev. B* **1977**, *15*, 2929–2942, doi:10.1103/PhysRevB.15.2929.

55. Allen, G.C.; Crofts, J.A.; Curtis, M.T.; Tucker, P.M.; Chadwick, D.; Hampson, P.J. X-Ray photoelectron spectroscopy of some uranium oxide phases. *J. Chem. Soc. Dalton Trans.* **1974**, 1296–1301, doi:10.1039/DT9740001296.
56. Seibert, A.; Gouder, T.; Huber, F. Reaction of neptunium with molecular and atomic oxygen: Formation and stability of surface oxides. *J. Nucl. Mater.* **2009**, *389*, 470–478, doi:10.1016/j.jnucmat.2009.03.002.
57. Seibert, A.; Gouder, T.; Huber, F. Interaction of PuO2 thin films with water. *Radiochim. Acta* **2010**, *98*, 647–654, doi:10.1524/ract.2010.1765.
58. Belli, K.M.; DiChristina, T.J.; Van Cappellen, P.; Taillefert, M. Effects of aqueous uranyl speciation on the kinetics of microbial uranium reduction. *Geochim. Cosmochim. Acta* **2015**, *157*, 109–124, doi:10.1016/j.gca.2015.02.006.
59. Regenspurg, S.; Schild, D.; Schäfer, T.; Huber, F.; Malmström, M.E. Removal of uranium(VI) from the aqueous phase by iron(II) minerals in presence of bicarbonate. *Appl. Geochem.* **2009**, *24*, 1617–1625, doi:10.1016/j.apgeochem.2009.04.029.
60. Missana, T.; García-Gutiérrez, M.; Fernńdez, V. Uranium (VI) sorption on colloidal magnetite under anoxic environment: Experimental study and surface complexation modelling. *Geochim. Cosmochim. Acta* **2003**, *67*, 2543–2550, doi:10.1016/S0016-7037(02)01350-9.
61. Petitto, S.C.; Tanwar, K.S.; Ghose, S.K.; Eng, P.J.; Trainor, T.P. Surface structure of magnetite (111) under hydrated conditions by crystal truncation rod diffraction. *Surf. Sci.* **2010**, *604*, 1082–1093, doi:10.1016/j.susc.2010.03.014.
62. Chadwick, D. Uranium 4f binding energies studied by X-ray photoelectron spectroscopy. *Chem. Phys. Lett.* **1973**, *21*, 291–294, doi:10.1016/0009-2614(73)80137-X.
63. Wersin, P.; Hochella Jr, M.F.; Persson, P.; Redden, G.; Leckie, J.O.; Harris, D.W. Interaction between aqueous uranium (VI) and sulfide minerals: Spectroscopic evidence for sorption and reduction. *Geochim. Cosmochim. Acta* **1994**, *58*, 2829–2843, doi:10.1016/0016-7037(94)90117-1.
64. Hennig, C.; Ikeda-Ohno, A.; Tsushima, S.; Scheinost, A.C. The sulfate coordination of Np(IV), Np(V), and Np(VI) in aqueous solution. *Inorg. Chem.* **2009**, *48*, 5350–5360. doi:10.1021/ic9003005
65. Husar, R.; Hübner, R.; Hennig, C.; Martin, P.M.; Chollet, M.; Weiss, S.; Stumpf, T.; Zänker, H.; Ikeda-Ohno, A. Intrinsic formation of nanocrystalline neptunium dioxide under neutral aqueous conditions relevant to deep geological repositories *Chem. Commun.* **2015**, *51*, 1301–1304. doi:10.1039/C4CC08103J
66. Cakir, P.; Eloirdi, R.; Huber, F.; Konings, R.J.M.; Gouder, T. Surface reduction of neptunium dioxide and uranium mixed oxides with plutonium and thorium by photocatalytic reaction with ice. *J. Phys. Chem. C* **2015**, *119*, 1330–1337, doi:10.1021/jp508239u.
67. Teterin, A.Y.; Maslakov, K.I.; Teterin, Y.A.; Kalmykov, S.N.; Ivanov, K.E.; Vukcevic, L.; Khasanova, A.B.; Shcherbina, N.S. Interaction of neptunyl with goethite (alpha-FeOOH), maghemite (gamma-Fe2O3), and hematite (alpha-Fe2O3) in water as probed by X-ray photoelectron spectroscopy. *Russ. J. Inorg. Chem.* **2006**, *51*, 1937–1944, doi:10.1134/s0036023606120151.
68. Cox, L.E.; Farr, J.D. 4f binding-energy shifts of the light-actinide dioxides and tetrafluorides. *Phys. Rev. B* **1989**, *39*, 11142–11145, doi:10.1103/PhysRevB.39.11142.
69. Yang, S.; Zhao, Y.; Tian, G. Np(v) complexation with carbonate in aqueous solutions studied by spectrophotometric titration at various temperatures. *Dalton Trans.* **2016**, *45*, 2681–2685, doi:10.1039/C5DT04447B.
70. Dong, W.; Brooks, S.C. Determination of the Formation Constants of Ternary Complexes of Uranyl and Carbonate with Alkaline Earth Metals (Mg2+, Ca2+, Sr2+, and Ba2+) Using Anion Exchange Method. *Environ. Sci. Technol.* **2006**, *40*, 4689–4695, doi:10.1021/es0606327.
71. Wander, M.C.F.; Kerisit, S.; Rosso, K.M.; Schoonen, M.A.A. Kinetics of triscarbonato uranyl reduction by aqueous ferrous iron: A theoretical study. *J. Phys. Chem. A* **2006**, *110*, 9691–9701.
72. García Flores, H.G.; Roussel, P.; Moore, D.P.; Pugmire, D.L. Characterization and stability of thin oxide films on plutonium surfaces. *Surf. Sci.* **2011**, *605*, 314–320, doi:10.1016/j.susc.2010.10.034.
73. Marquardt, C.M.; Seibert, A.; Artinger, R.; Denecke, M.A.; Kuczewski, B.; Schild, D.; Fanghänel, T. The redox behaviour of plutonium in humic rich groundwater. *Radiochim. Acta* **2004**, *92*, 617–623, doi:10.1524/ract.92.9.617.55007.